

Reevaluating carbon fluxes in subduction zones, what goes down, mostly comes up

Peter B. Kelemen^{a,1} and Craig E. Manning^{b,1}

^aDepartment of Earth & Environmental Sciences, Columbia University, Lamont–Doherty Earth Observatory, Palisades, NY 10964; and ^bDepartment of Earth, Planetary, and Space Sciences, University of California, Los Angeles, CA 90095

This contribution is part of the special series of Inaugural Articles by members of the National Academy of Sciences elected in 2014.

Contributed by Peter B. Kelemen, April 23, 2015 (sent for review August 7, 2014; reviewed by Jay J. Ague, James Connolly, Rajdeep Dasgupta, and Dimitri Sverjensky)

Carbon fluxes in subduction zones can be better constrained by including new estimates of carbon concentration in subducting mantle peridotites, consideration of carbonate solubility in aqueous fluid along subduction geotherms, and diapirism of carbon-bearing metasediments. Whereas previous studies concluded that about half the subducting carbon is returned to the convecting mantle, we find that relatively little carbon may be recycled. If so, input from subduction zones into the overlying plate is larger than output from arc volcanoes plus diffuse venting, and substantial quantities of carbon are stored in the mantle lithosphere and crust. Also, if the subduction zone carbon cycle is nearly closed on time scales of 5–10 Ma, then the carbon content of the mantle lithosphere + crust + ocean + atmosphere must be increasing. Such an increase is consistent with inferences from noble gas data. Carbon in diamonds, which may have been recycled into the convecting mantle, is a small fraction of the global carbon inventory.

carbon cycle | subduction | aqueous geochemistry | metasediment diapirs | peridotite carbonation

Flux of carbon that is returned to Earth's interior by subduction is important but poorly constrained. There have been several recent reviews of the subduction carbon cycle (1–8). These studies estimate that about half of subducted carbon is removed from the downgoing plate beneath forearcs and arcs and returned to Earth's surface [40% in Gorman et al. (8); 20–80% in Dasgupta and Hirschmann (1); and 18–70% in Johnston et al. (6)].

Key carbon reservoirs and transport mechanisms can now be better quantified. These include carbon concentration ([C]) in altered mantle lithologies (this paper plus refs. 9 and 10), carbon solubility in aqueous fluids at subduction zone conditions (this paper plus refs. 11 and 12), the volume of altered peridotites in subducting oceanic plates (especially ref. 13), the volume of altered peridotite in the mantle wedge, and the nature of meta-sedimentary diapirs rising from subducting crust (14).

In this paper, we reevaluate carbon fluxes in several tectonic settings. We start with carbon uptake during hydrothermal alteration near midocean ridges, followed by an estimate of carbon addition during alteration of shallow mantle peridotite at the “outer rise,” where subducting oceanic plates bend before subduction. We then consider carbon transfer in fluids and melts derived from the subducting plate. Finally, we review carbon outputs from arc volcanoes and via diffuse venting.

Carbon Uptake During Hydrothermal Alteration of Basaltic Oceanic Crust: 22–29 Mt C/y

Following Alt and Teagle (15), we compiled data on [C] in altered oceanic crust ([Dataset S1](#); also see [SI Text](#)). [C] is now thought to be higher in volcanic rocks and lower in gabbros. These differences offset each other, so our estimate of 500–600 ppm carbon in oceanic crust agrees with Alt and Teagle. Oceanic plates are consumed at an average of ~ 0.05 m/y along the $\sim 44,500$ -km length of global subduction zones (4). These values and [C] in altered oceanic crust yield a carbon flux of 22–29 Mt C/y ([Dataset S2](#)).

Seismic data and seafloor outcrops imply that 5–15% of oceanic crust that formed at slow- and ultraslow-spreading ridges is composed of altered mantle peridotite, with the extent of serpentinization varying from $\sim 100\%$ at the seafloor to $\sim 0\%$ at ~ 7 km depth (16, 17). Because slow- and ultraslow-spreading crust is formed at $\sim 30\%$ of midocean ridges (18, 19), crust composed of altered peridotite is 1–4% of the total, and not a significant part of the global carbon budget. However, almost all available data on [C] in altered peridotite come from seafloor samples.

We compiled data on [C] in altered mantle peridotite from seafloor and ophiolite samples ([Dataset S3](#)). After eliminating outliers—six samples with much higher [C] than the other 223 samples—these data yield an average of 681 ± 45 ppm carbon (1σ). This is consistent with studies of metamorphosed seafloor peridotites (3, 20–22). Fig. 1 illustrates the relationship of [C] versus H₂O content in altered peridotites. In turn, we relate this to the volume proportion of serpentine because almost all H₂O in these samples is in serpentine.

Subduction of Carbon-Bearing Sediments: 13–23 Mt C/y

[C] in oceanic sediments was reviewed by Rea and Ruff (23), Plank and Langmuir (24), and Plank (25). These studies do not fully account for organic carbon, particularly in pelagic sediments and turbidites. Where measured (e.g., ref. 26), organic carbon averages around 1 wt% in hemipelagic ooze that is nearly free of carbonate. Samples of such sediments in which [C] was not measured were assumed to be carbon free. On this basis, and the observation that these lithologies are more common than

Significance

This paper reviews carbon fluxes into and out of subduction zones, using compiled data, calculations of carbon solubility in aqueous fluids, and estimates of carbon flux in metasedimentary diapirs. Upper-bound estimates suggest that most subducting carbon is transported into the mantle lithosphere and crust, whereas previous reviews suggested that about half is recycled into the convecting mantle. If upper-bound estimates are correct, and observed output from volcanoes and diffuse outgassing is smaller, then the mantle lithosphere is an important reservoir for carbon. If the subduction carbon cycle remains in balance, then outgassing from ridges and ocean islands is not balanced, so that the carbon content of the lithosphere + ocean + atmosphere has increased over Earth history.

Author contributions: P.B.K. and C.E.M. designed research, performed research, contributed new reagents/analytic tools, analyzed data, and wrote the paper.

Reviewers: J.J.A., Yale University; J.C., ETH Zurich; R.D., Rice University; and D.S., Johns Hopkins University.

The authors declare no conflict of interest.

Freely available online through the PNAS open access option.

¹To whom correspondence may be addressed. Email: peterk@ldeo.columbia.edu or manning@epss.ucla.edu.

This article contains supporting information online at www.pnas.org/lookup/suppl/doi:10.1073/pnas.1507889112/-DCSupplemental.

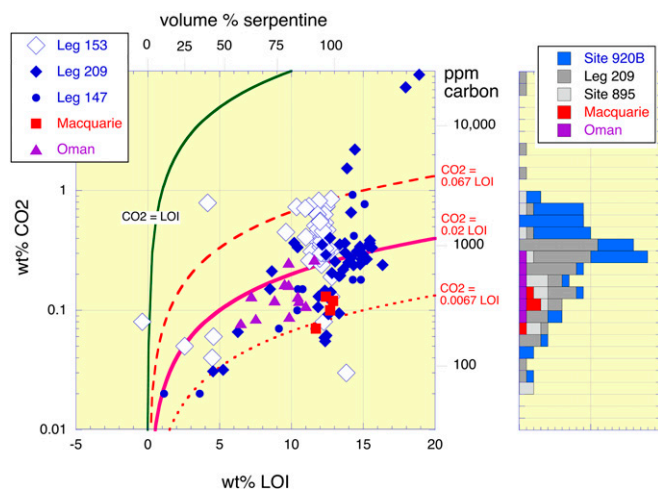


Fig. 1. Relationship of loss-on-ignition (LOI) to $[CO_2]$ (left axis) and $[C]$ (right axis) in altered mantle peridotites from ophiolites and midocean ridges. Top scale translates LOI to volume percent serpentine, assuming LOI is mainly H_2O in serpentine with a density of $2,485 \text{ kg/m}^3$, and prealteration density is $3,300 \text{ kg/m}^3$. Contours show linear relationships between LOI and $[CO_2]$, with intercept = 0 and slopes given on the left axis in red. Data sources in [Dataset S3](#).

carbonates in subducting sediments (25), we retain the lower-bound flux of 13 Mt C/y in subducting sediments (1), but revise the upper bound from 17 Mt C/y to 23 Mt C/y (also see ref. 27).

Our analysis focuses on steady-state fluxes of carbon subducting to depths of $\sim 300 \text{ km}$ on time scales of $\sim 10 \text{ Ma}$. Changing subduction rates, sedimentation rates, bottom water temperature, and changing oxidation states in the atmosphere and oceans, could have led to considerable variability in the nature and flux of subducting sedimentary carbon during Earth history (e.g., ref. 6). A relatively recent, significant factor was the mid-Mesozoic shift from formation of shelf carbonates to deposition of pelagic carbonates in the deep ocean (e.g., refs. 28–30). This may have changed the nature of carbon subduction, from periodic fluxes during continental collisions to a closer approach to steady state. Fluxes of subducting carbon also varied due to changes in the length and convergence rate of subduction zones worldwide (e.g., ref. 31). As with the possible temporal variability of $[C]$ in oceanic crust, this is an important topic for future, comprehensive study.

Carbon Uptake at the Outer Rise: 4–15 Mt C/y

The outer rise is a trench-parallel, bathymetric high caused by bending and faulting of oceanic plates before subduction (32, 33). Seismic studies show that active faults extend into the mantle at and near the outer rise, associated with serpentinization (*SI Text*). At the outer rise adjacent to the Central American subduction zone, a layer of mantle peridotite $\sim 10 \text{ km}$ thick undergoes ~ 10 – 30% serpentinization (13). Uncertainty in the proportion of serpentinization arises mainly from systematic along-strike variation in the nature of the subducting oceanic plate, as also seen for the Alaska subduction zone by Shillington et al. (34).

A preliminary assessment of carbon uptake can be made by assuming that $[C]$ in serpentinized peridotites at the outer rise is similar to that of seafloor peridotites. Thus, for example, we infer that $[C]$ in the upper 10 km of the mantle section of a subducting oceanic plate with 10% serpentine is $10\% \times 681 \pm 45 \text{ ppm}$. These assumptions imply that outer-rise alteration takes up 4 – 15 Mt C/y . Our estimates are similar to those of Dasgupta (ref. 2; 1 – 10 Mt C/y) and Alt et al. (ref. 3; 0.16 – 1.9 Mt C/y) and, although clearly preliminary, show that mantle alteration at the outer rise may be significant in the global carbon cycle.

Carbon Transfer into the Leading Edge of the Mantle Wedge ($<300 \text{ }^\circ\text{C}$ and $<1 \text{ GPa}$): 0.1 – 1.3 Mt C/y

Prior studies inferred that there is no significant transfer of carbon from the footwall into the hanging wall at subduction zone depths less than 60 – 70 km (e.g., refs. 1, 8, and 35). However, the presence of fully carbonated peridotites composed of magnesite + quartz and dolomite + quartz (“listvenites”) in ophiolites thrust over metasediments suggests substantial carbon transfer at low temperatures (T) (36). For ~ 15 – 20 million years starting at $\sim 96 \text{ Ma}$, the Samail ophiolite of Oman was thrust over oceanic crust and sediments (37, 38). Listvenites formed at $\sim 100 \text{ }^\circ\text{C}$ in partially serpentinized peridotite within 500 m of exposed contacts with footwall rocks. Their Rb/Sr age of $97 \pm 17 \text{ Ma}$ indicates formation during ophiolite emplacement. The thickest mapped layer contains ~ 1 billion tons of CO_2 . Samail listvenites have higher $^{87}\text{Sr}/^{86}\text{Sr}$ than Cretaceous to modern seawater, implying that Sr was derived from underlying sediments containing radiogenic $^{87}\text{Sr}/^{86}\text{Sr}$, and we infer that sediment-derived fluid was also the source of the CO_2 and Ca in the listvenites (36). At $\sim 100 \text{ }^\circ\text{C}$ along a shallow subduction zone geotherm of 5 – $15 \text{ }^\circ\text{C/km}$, listvenite formation occurred at 7 – 20 km (0.2 – 0.6 GPa) based on thermal models of subduction zones (e.g., refs. 39 and 40), consistent with the thickness of the Samail ophiolite (5 – 7 km oceanic crust + up to 15 km of mantle peridotite).

Similar listvenites, some formed at higher T , are found elsewhere at and near the contact where peridotites are thrust over metasediments (*SI Text*). If such layers form above 1 – 10% of subduction zones worldwide, with an average thickness of 10 – 100 m , this corresponds to transfer of 0.06 – 6 Mt C/y into the leading edge of the mantle wedge. These values are highly uncertain, but we prefer intermediate values based on thermodynamic constraints on carbon flux out of subducting sediments in this depth interval (last paragraph of this section).

Seismic studies of subduction zones (*SI Text*) generally report a large proportion of serpentine in the leading edge of the mantle wedge, extending from the crust–mantle boundary to the arc–forearc transition (where heat flow abruptly increases away from the trench). [Dataset S4](#) provides a compilation of estimates for the proportion of serpentine in these regions, and for the volume and mass of the serpentinized part of the wedge.

Intraoceanic subduction zones have thinner crust and more peridotite in the leading edge of the overthrust plate. Hydration of this peridotite at low T forms chrysotile + lizardite serpentine polytypes (40). At greater depths, the higher- T serpentine polytype, antigorite, is stable. Formation of antigorite may be geochemically very different from low- T alteration of peridotite near the seafloor. Thus, our data on $[C]$ in seafloor and ophiolite peridotite samples (*Carbon Uptake During Hydrothermal Alteration*) may have little bearing on $[C]$ in antigorite peridotites. Nevertheless, there are no other data on $[C]$ in this potentially important reservoir. In any case, the regions where antigorite could be stable comprise less than 33% of the forearc mantle, worldwide. Based on the data in [Datasets S3](#) and [S4](#), we estimate carbon flux associated with serpentinization in the leading edge of the mantle wedge to be 0.2 – 1.3 Mt C/y .

Thermodynamic calculations yield carbon solubilities of 50 – 500 ppm in aqueous fluids saturated in carbonate-bearing mudstone compositions in the pressure–temperature (PT) range for Oman listvenites (36). A combination of compaction (e.g., ref. 41) and clay dehydration (e.g., ref. 42) could produce ~ 14 – $44 \text{ wt}\%$ aqueous fluid from carbonate-bearing, clay-rich sediments in this depth interval, yielding an upper bound of $\sim 1 \text{ Mt C/y}$. Larger fluxes of carbon could result from focusing of aqueous fluids from deeper metamorphic dehydration reactions.

Carbon Transfer in Greenschist and Blueschist Facies (~ 300 – $550 \text{ }^\circ\text{C}$, 0.5 – 2 GPa): 0.001 – 0.6 Mt C/y

We were unable to find $[C]$ data for metaperidotites believed to represent the “cold nose” of the mantle wedge. Many metaperidotites recording subduction zone metamorphism are inferred to represent subducted, seafloor peridotites that were serpentinized near slow-spreading midocean ridges. This is the case for

most or all such samples analyzed for bulk [C] (3, 21, 22). If these interpretations are correct, then [C] in these samples predates subduction, and provides little information on transfer of carbon from the footwall into the mantle wedge. Although they do not report [C], several other studies describe carbonate minerals, hydrocarbon-bearing fluid inclusions and/or graphite, in hanging-wall peridotites (*SI Text*). Carbon-bearing phases are also reported in talc and/or chlorite schists inferred to represent hanging-wall peridotites modified by mechanical mixing and chemical reaction metasediment and metabasalt (*SI Text*).

Studies of blueschist facies mélanges on Santa Catalina Island, CA, provide particularly comprehensive data (e.g., ref. 43 and references therein). Graphite and/or carbonate minerals are common in the matrix of blueschist and greenschist facies metasediments, and locally present in lawsonite–albite, blueschist and greenschist facies metasediments, and mafic rocks (44). They are major phases in hybridized metaperidotites and cross-cutting veins in 9 of 14 samples from lawsonite–albite facies, 3 of 18 samples from blueschist facies, and 2 of 11 samples from greenschist facies, and are minor phases in 9 other samples (45).

Our reconnaissance sampling at Santa Catalina revealed extensive zones of talc–carbonate rocks composed of calcite + dolomite + talc near the Pacific coast (Fig. 2). Our preliminary observations suggest that talc–carbonate rocks comprise 5–10% of the rock volume in this area. We hypothesize that they were not previously reported because they weather readily, and rarely form rocky outcrops. Talc–carbonate rocks, like listvenites, form via extensive reaction of CO₂-bearing aqueous fluids with mantle peridotite (e.g., refs. 46 and 47). In Oman and in several Canadian localities, talc–carbonate lithologies formed at ~250–300 °C (*SI Text*).

Ague and Nicolescu (48) recently highlighted the importance of CaCO₃ dissolution by aqueous fluids associated with blueschist facies metamorphism. We can make quantitative estimates of carbon solubility in aqueous fluids under these conditions using new data on the solubility of CaCO₃ minerals in aqueous fluids as a function of *P*, *T*, and salinity (reviews in refs. 11 and 12). We use data from Sverjensky et al. (49) and Facq et al. (50) for aqueous species to compute the solubility of stable CaCO₃ polymorphs as a function of *P* and *T* (Fig. 3). The solubility of CaCO₃ in pure H₂O, and in H₂O saturated with model sediment (K-feldspar + muscovite ± quartz) and model peridotite (forsterite + enstatite) are nearly identical because the dominant aqueous

electrolytes contributed by the silicate assemblages (K⁺, Mg⁺², MgOH⁺) are present in low concentrations relative to solutes from CaCO₃ dissolution.

Fig. 3A shows that carbon solubility in fluids equilibrated with CaCO₃-bearing assemblages at ~300–550 °C and 0.5–2 GPa ranges from ~10 ppm to 2,000 ppm. If metamorphic reactions in this *PT* range generate 1–4 wt% aqueous fluid, this corresponds to global fluxes of 0.001–0.6 Mt C/y. These are probably minimum values. CaCO₃ solubility increases at a given *P* and *T* with decreasing pH associated with abundant charged aqueous clusters (e.g., ref. 12), with addition of NaCl (51), and decreasing fO₂ (52), which are all likely in subduction zones.

Cook-Kollars et al. (53) studied carbon mass transfer in blueschist facies metasediments in the Italian Alps. They found limited evidence for large-scale carbon loss due to interaction with aqueous fluids derived from deeper in the subducting plate, consistent with the estimates above. A caveat is that such studies potentially involve a sampling bias because it is difficult to identify former carbonate-bearing metasediments from which the original carbonate minerals have been entirely or extensively removed by dissolution.

Carbon Transfer at High-Grade, Subsolvus Conditions (~550–800 °C, 2–6 GPa): 4–58 Mt C/y

As for lower-grade rocks described in the previous section, data on [C] in identified, mantle wedge peridotites in eclogite and ultra-high pressure (UHP) metamorphic facies are rare or absent. However, the presence of carbonate minerals, graphite, diamond and/or carbon-rich fluid inclusions is increasingly being noted in mantle wedge peridotites formed at eclogite and UHP facies (*SI Text*). Carbon-bearing phases are typically associated with amphibole- and/or phlogopite-bearing mineral assemblages, with hydration and carbonation attributed to input from subduction zones. Most identified mantle wedge localities were emplaced in continental collision zones rather than typical intraoceanic subduction zones. Although they provide information on carbon transfer, they do not yield direct constraints on fluxes during subduction of oceanic crust.

A notable exception is the Sanbagawa metamorphic belt, particularly in and around the Higashi-Akaishi garnet peridotite body, which overlies and was metamorphosed along with eclogite facies metasediments derived from the subducting Pacific plate (refs. 54 and 55 and *SI Text*). Olivine in the peridotites contains carbonate mineral inclusions and carbon-rich fluid inclusions (56–58). The Sanbagawa metasediments are less dense than peridotite at the same *PT* conditions. This buoyancy contrast is thought to have driven ascent of the lithologic package—including small bodies of peridotite—after high-*P* metamorphism (59). The metasediments include marbles that could have provided a source of dissolved carbon in aqueous fluids. On a recent trip to this area, we found that the peridotites include olivine–carbonate veins (Fig. 2), although the *PT* and timing of vein formation are not known.

Calculated carbon solubility in fluids equilibrated with metasediment at eclogite and UHP conditions could range from 0.1 to 3 wt% or more (Fig. 3). This is also the case for fluid equilibrated with metabasalt and serpentinite. Such high solubilities are consistent with [C] in fluid inclusions in diamond-bearing UHP metasediments (60). Dehydration of metasediments and metabasalts in this *PT* range could yield a few weight percent of fluid. Extraction of 1 wt% fluid corresponds to a global flux of 0.1–2.2 Mt C/y.

In addition, dehydration of serpentinites in the subducting mantle lithosphere supplies aqueous fluid that fluxes the overlying lavas and sediments (e.g., refs. 8, 61, and 62). The solubility of carbon in carbonate-saturated fluids derived from antigorite breakdown in peridotite is ~5,000 ppm (Fig. 3). On average, fully serpentinitized peridotites have ~680 ppm carbon and ~14 wt% H₂O in serpentine (*Carbon Uptake During Hydrothermal Alteration*). Thus, there is sufficient H₂O to dissolve all of the carbonate minerals in the shallow mantle (0.14 × 5,000 = 700 ppm).



Fig. 2. Examples of carbon-bearing rocks formed in subduction zones. (*Top Left*) Listvenites about 500 m above the basal thrust of the Samail ophiolite in Oman (36). (*Top Right*) Talc–carbonate rock near Little Harbor, Santa Catalina, CA. (*Bottom Left*) Marble in eclogite facies metasediments underlying the Higashi-Akaishi mantle peridotite, Japan. (*Bottom Right*) Magnesite-bearing dunite vein cutting chromite band in the Higashi-Akaishi peridotite.

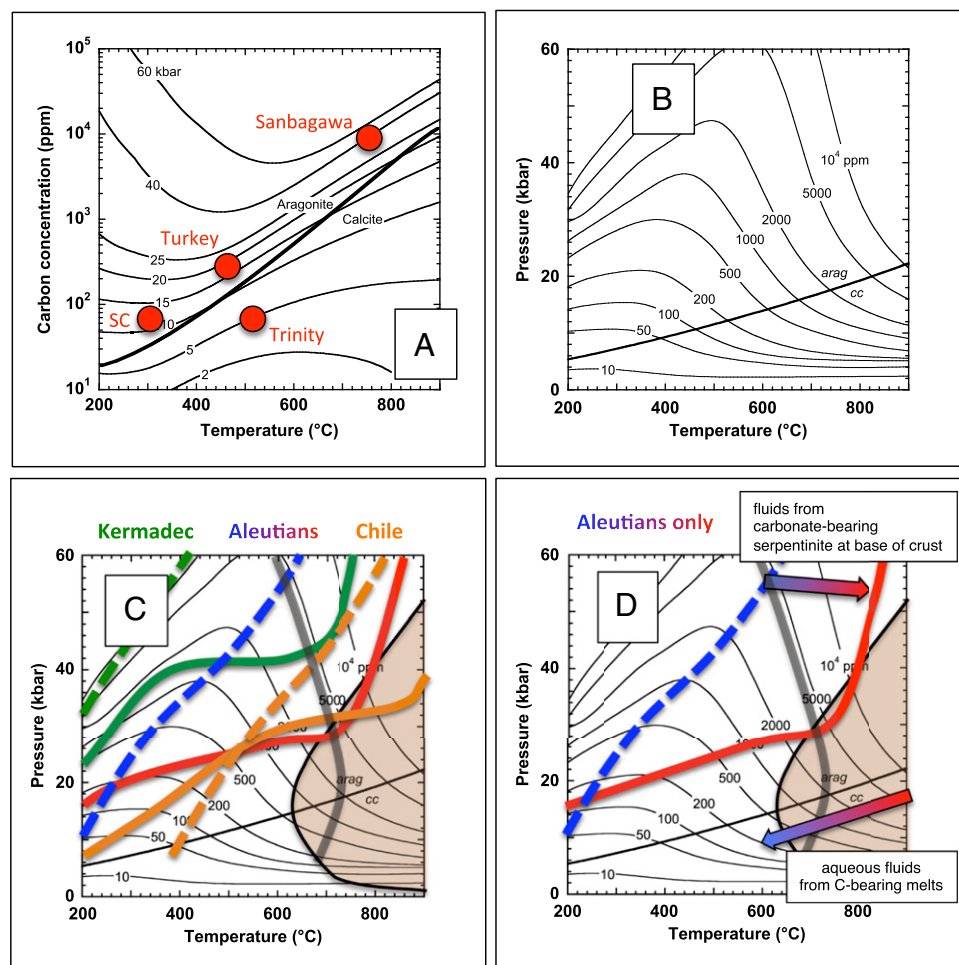


Fig. 3. Solubility of CaCO_3 in aqueous fluids (see *SI Text* for calculation methods and references). (A) Isobars of CaCO_3 solubility as a function of T . Red circles indicate PT solubility conditions for Santa Catalina; the basal thrust of the Trinity peridotite; lawsonite blueschists; and eclogite to UHP metamorphic terrains such as western Norway and the Higashi-Akaishi peridotite, Japan. (B) Contours of $[C]$ in parts per million for aqueous fluids saturated in CaCO_3 as a function of P and T . (C) B overlain by 25 \times subduction zone geotherms of Syracuse et al. (39). Dashed lines, base of subducting oceanic crust; solid lines, top of subducting volcanics and sediments; green, Kermadec; blue and red, Aleutians; orange, southern Chile. Solid gray curve indicates stability limit of serpentine (118). Orange field indicates PT conditions above the fluid-saturated solidus for metabasalt and metasediment (69). (D) B with Aleutian geotherms. Upper arrow, PT trajectory for fluids produced by serpentinite dehydration; lower arrow, PT trajectory for fluids rising into the mantle lithosphere and crust.

These fluids heat as they rise through the subducting plate, so carbon solubility will increase to several weight percent (Fig. 3). Even if they are close to carbonate saturation when generated, they can dissolve several weight percent carbon when they reach the top of the subducting plate. Reaction of carbonate-bearing metasediments and metabasalts with 10 wt% aqueous fluid derived from serpentinite dehydration could yield a global flux as high as 22 Mt C/y, provided that sufficient carbonate was present within the metasediments.

Carbonate dissolution in such fluids represents an additional carbon flux that must be added to the flux derived from models that do not account for mineral dissolution (8, 35, 63, 64). Their only source of carbon is the forward progress of decarbonation reactions (e.g., aragonite + quartz = wollastonite + CO_2); all minerals are assumed to be perfectly insoluble. However, Fig. 3 demonstrates that carbonate mineral solubility is actually quite high in H_2O -rich fluid at subduction zone conditions.

The open system calculations of Gorman et al. (8) afford the best estimate of carbon flux derived solely from decarbonation reactions in the absence of mineral dissolution. Their distillation model yields a global flux of about 4 Mt C/y from the subducting plate into the mantle wedge and provides a lower bound for carbon flux from the subducting plate in eclogite and

UHP metamorphic facies. Their fluxed model, in which H_2O -rich serpentinite-derived fluid drives decarbonation reactions, yields a global flux of ~ 37 Mt C/y. We add the upper-bound dissolution and metamorphic fluxes of 22 Mt C/y to yield an upper bound of ~ 59 Mt C/y from the subducting plate in eclogite and UHP facies.

Mineral solubilities in H_2O are lowered by addition of CO_2 derived from decarbonation reactions. However, the combination of low CO_2 mole fractions of subduction zone fluids [<0.2 (8)] and the relatively minor effect on H_2O dielectric constant (65) will conspire to maintain high carbonate mineral solubilities, even in rocks undergoing decarbonation reactions.

These considerations have four important consequences for carbon mass transfer in subduction zones.

- Fluid derived from serpentinite dehydration at eclogite-facies conditions can dissolve all of the carbonate formed in the shallow mantle before subduction.
- Fluid derived from serpentinites can dissolve much of the carbonate in subducting basalts and sediments (below the aqueous fluid-saturated solidus), and drive metamorphic decarbonation reactions, potentially removing all carbon from the subducting plate.

- iii) Lithologic contrasts are unlikely to cause significant CaCO_3 precipitation due to the CaCO_3 solubility in pure H_2O , model metasediment, and model peridotite. The main controls on subsolidus CaCO_3 mobility are the PT gradient along the fluid flow path, and changes in salinity or $f\text{O}_2$.
- iv) If they do not cause partial melting, carbon-bearing aqueous fluids that rise within the mantle will remain undersaturated with CaCO_3 as they heat within the hot corner of the wedge [high dT/dP (e.g., refs. 39 and 40)]. At shallower levels, decompression and cooling of rising fluids in the lithosphere will cause gradual precipitation of carbonate over a range of depths. Carbonate precipitation will occur mainly in serpentine-free peridotites at $>600^\circ\text{C}$, assuming local equilibrium.

Carbon Transfer in Hydrous Melts Near the Aqueous Fluid-Saturated Solidus: Continues Mass Transfer from Aqueous Fluids

The H_2O -saturated solidus for metasediments and metabasalts extends almost linearly from $\sim 625^\circ\text{C}$ at 2 GPa to $\sim 925^\circ\text{C}$ at the second critical endpoint near 5.5 GPa (Fig. 3C and *SI Text*). When there is appreciable dissolved CO_2 , the solidus shifts to higher T ($\sim 800^\circ\text{C}$ at 3 GPa to 925°C at 5 GPa).

Thermal models indicate that the tops of some subducting plates attain temperatures above the fluid-saturated solidus, whereas others do not. There is a steep thermal gradient in the top of the subducting plate so that in all but the hottest subduction zones, most of the subducting plate is below the aqueous fluid-saturated solidus at 2–6 GPa (Fig. 3). In subduction zones in which fluid-saturated anatexis occurs, the fluid—which at any given time is unlikely to comprise more than 1 wt% of a given rock system—will dissolve in near-solidus, hydrous silicate melt. Near the solidus, this will produce a small degree melt with ~ 30 wt% H_2O (66, 67). Dissolved CO_2 in the fluid will thus be diluted by $\sim 33\%$ in the melt compared with the fluid. Dissolution of carbonate-saturated fluid with ~ 3 wt% carbon (~ 11 wt% CO_2) would yield about 4 wt% CO_2 in the melt, less than or equal to solubility of CO_2 in silica-rich melts at ≥ 3 GPa (68). The solubility of CO_2 in melt and aqueous fluid becomes continuous at the second critical endpoint [$\sim 925^\circ\text{C}$, 5.5 GPa (69)]. Above this P and T , CO_2 solubility in supercritical liquid is likely to be ~ 5 wt% or more.

With increasing T above the solidus, the melt fraction will rise, and $[\text{CO}_2]$ will fall to values well below the concentration required for CO_2 saturation, allowing continued dissolution/melting of residual carbonate. Moreover, incremental delivery of small amounts of fluid, driving distillation of fluid-saturated partial melt, will gradually raise the time-integrated degree of melting and exhaust residual carbonate in most metasedimentary assemblages (68), except for carbonate-rich lithologies such as marbles.

Carbon Transfer via Fluid-Absent Melting: Important only in the Hottest Subduction Zones

Above 800–1,050 $^\circ\text{C}$ at 2–5 GPa, remaining carbonate- and hydrous silicate-bearing, subducting lithologies (*SI Text*) will undergo fluid-undersaturated partial melting. Liquids will be silicate melt compositions, potentially rich in CO_2 , that will rise farther into the mantle wedge where they will cause additional flux melting of peridotite (refs. 70, 71, and 72 and references therein). Once these compositions heat beyond, e.g., 900–1,050 $^\circ\text{C}$ at 3 GPa (figure 8 in ref. 70), no residual solid carbonates are likely to remain. However, such high T/P conditions are unlikely to be attained in all but the hottest subduction zones.

Carbon Transfer via Buoyant Diapirs: Much of What's Left

Under H_2O -poor conditions, some metabasalt and metasediments will remain below their solidi along subduction geotherms well into the upper mantle (2). However, most metasediments are $>200\text{ kg/m}^3$ less dense than peridotite at subduction zone conditions. Kelemen et al. (73) and Behn et al. (14) predicted that, when they reach 700–900 $^\circ\text{C}$ at 75–250 km depth, slab top

metasediment layers that are >100 m thick and $\sim 200\text{ kg/m}^3$ less dense than peridotite would form diapirs and rise into the mantle wedge. Marbles and carbonate-bearing metapelites are likely to be included in such diapirs (14, 74, 75). Hybrid subduction mélanges formed by mechanical mixing and chemical interaction are also likely to be buoyant, and to rise through the subduction channel or mantle wedge (76). Such mélanges can include substantial carbonate (*Carbon Transfer in Greenschist and Blueschist Facies*).

In subducting sedimentary sections worldwide, carbonate layer thicknesses commonly exceed 100 m, and carbon-bearing minerals are abundant within packages of low-density sediments whose average thickness is >500 m (25). Thus, most of the carbon remaining in subducting metasediments—up to 47 wt% of the total carbon in the subducting plate—is susceptible to transport through the mantle wedge in diapirs. Only thin metasedimentary layers and remaining, undissolved carbonate alteration in metabasalts and metaperidotites may pass this depth and be directly recycled into the convecting mantle.

The fate of metasedimentary diapirs within the mantle is speculative but important. The fluid-absent solidi for Ca and/or Mg carbonates are at more than 1,400–1,500 $^\circ\text{C}$ at mantle wedge pressures to ≥ 200 km depth, so the interiors of pure marble diapirs will remain solid (e.g., ref. 77). However, along the margins or rising diapirs, carbonate minerals + olivine + pyroxenes at $T > 1,250^\circ\text{C}$ will produce CO_2 -rich melts (e.g., refs. 78 and 79).

Metasediments, including calc-silicates, that pass through the hot core of the mantle wedge will undergo high degrees of fluid-absent partial melting (*SI Text*). Certain xenoliths may represent the residue of such melting (80). The resulting melts will react with peridotite along the margins of partially molten diapirs. Where the melt–rock ratio is high and melts are hydrous, this could produce primitive andesites (81); at small melt–rock ratios and low H_2O contents, the products are likely to be alkali basalts (70, 71). These melts will rise into the mantle lithosphere.

Thus, it is likely that almost all of the carbon in metasedimentary diapirs is transferred into carbonate-bearing silicate melts in the hot core of the mantle wedge. Melts from diapirs, plus slab-derived melts, plus fluid-fluxed melts of the mantle—and any remaining solid, marble cores—will rise into the mantle lithosphere and lower crust. Where they rise into the mantle at $<1,250^\circ\text{C}$, the melts will encounter the shelf in the carbonated peridotite solidus—extending from $\sim 1,000^\circ\text{C}$ at 2 GPa to $1,250^\circ\text{C}$ at 1 GPa—where CO_2 -rich fluid + olivine + pyroxene (+ garnet or spinel) become stable at low P with respect to CO_2 -rich melt (Fig. 4). For melt with abundant dissolved H_2O and CO_2 , this will produce hydrous melts, some crystallization, and CO_2 -rich fluid. For melts with little or no H_2O , this will cause extensive crystallization and produce abundant CO_2 -rich fluid.

The solubility of carbon in aqueous fluids cooling from 900 $^\circ\text{C}$ to 600 $^\circ\text{C}$ and decompressing from 2 GPa to 1 GPa drops by a factor of ~ 100 . Large amounts of carbonate would be precipitated from such rising fluids. Additional CO_2 -rich fluid could emerge in volcanic arcs, contribute to diffuse emissions in regions flanking arc volcanoes, and/or form carbonate minerals in the lower crust (see next three sections). They could also form multicomponent brines that contribute to lower crustal granulite metamorphism (82–84).

In all of these scenarios, most of the CO_2 in metasedimentary diapirs would be transferred into the mantle lithosphere, arc crust, and/or ocean and atmosphere, instead of being transferred to the global, convecting mantle.

Output from Arc Volcanoes: 18–43 Mt C/y

Reviews of gas fluxes from arc volcanoes (5, 63, 85) yield bounds on emissions from arc volcanoes from 18 Mt C/y to 43 Mt C/y, based on direct measurements of SO_2 concentration and flux in volcanic plumes, together with observed CO_2/SO_2 ratios in gases and fluids, and/or somewhat more indirect estimates of ^3He flux, together with observed $^3\text{He}/\text{CO}_2$ ratios in gases, fluids, and volcanic glass. Direct measurements of CO_2 output from volcanoes are few. We expect that this will change soon, yielding better constraints. Burton et al. (5) emphasized that their estimate was

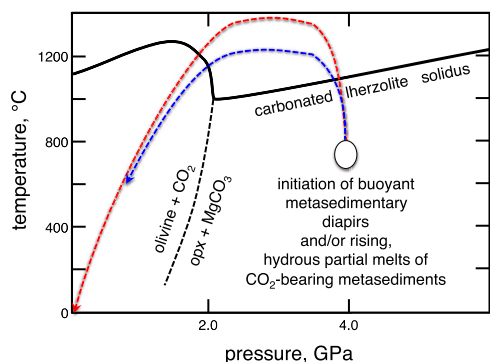


Fig. 4. *PT* trajectory for partial melts of subducting material and for buoyant diapirs. Melting of metabasalt and most metasediments, and melting along peridotite–marble contacts, will produce CO₂-bearing silicate melt. Reaction of these melts with peridotite will produce a range of CO₂+H₂O-bearing liquids from andesite to alkali basalt to carbonatite. CO₂-rich, H₂O-poor melts will crystallize and evolve CO₂-rich fluid at the carbonated lherzolite solidus (refs. 79 and 119 and additional references in *SI Text*). Hydrous melts will exsolve CO₂-rich fluids. Remaining melts and fluids will ascend past the carbonated lherzolite solidus and form carbon-bearing minerals in the mantle lithosphere and crust.

higher than that of Hilton et al. (85) and other recent reviews because of improving data quality and data density.

The source of CO₂ in arc volcano emissions can be ambiguous. Where CO₂ contents correlate with ³He, it is inferred that most of the CO₂ is introduced from the mantle into the base of arc crust. Where CO₂ and ³He are correlated, and ³He/CO₂ ratios are lower than in other tectonic settings, and/or where δ¹³C reflects input of nonmantle carbon, this is ascribed to recycling of carbon from subducting sediment and altered oceanic crust. However, arc volcanoes—particularly in continental arcs—may also emit CO₂ added to magmas during metamorphism of carbon-bearing lithologies within the crust (31).

CO₂ contents in melt inclusions in phenocrysts in arc lavas can be used to place lower bounds on CO₂ in parental magmas passing from the mantle into arc crust, as reviewed by Wallace (7). However, because the extent of prior degassing of CO₂ from decompressing melts currently cannot be determined with confidence, melt inclusion data have little utility in estimating an upper bound for magmatic input of CO₂ into arc lithosphere (e.g., ref. 86). Wallace (7) and Blundy et al. (86) arrive at similar estimates for CO₂ contents in primitive magmas passing from the mantle into arc crust. However, the estimate of Wallace was derived using inferred arc magma fluxes together with the volcanic CO₂ flux estimated by Hilton et al. (85), so these values are not independent. The estimate of Blundy et al. is based on the assumption that observed andesites are produced by 80% crystal fractionation from parental basalts, which could be too high; for example, using a value of 40% crystal fractionation would increase the estimated magmatic CO₂ flux by a factor of 2 compared with that of Hilton et al.

Additional studies of ³He/CO₂ are warranted to separate subduction zone versus arc crust contributions to CO₂ in arc volcanoes. Meanwhile, available results seem to indicate that most CO₂ emerging from arc volcanoes is derived from recycling of subducted CO₂. Estimates of CO₂ in parental magmas, before crystal fractionation, need to be refined.

Diffuse Outgassing of Carbon at Forearcs and Arcs: 4–12 Mt C/yr or More

Diffuse outgassing of subducted carbon as CO₂, methane, and other hydrocarbons could be an important part of the global carbon budget (5, 63, 87). However, even the most up-to-date reviews reflect measurements on a large range of scales that make it difficult to extract global estimates. We focus here on diffuse outgassing of CO₂ in arcs (forearc, arc, backarc). Evidence for such output is abundant. Haggerty and coworkers (ref. 88 and *SI Text*) first documented carbonate chimneys and authigenic carbonate deposited by fluids from subducting sediment and oceanic crust at and near seamounts in the Mariana and Bonin forearcs. Fryer and coworkers subsequently found

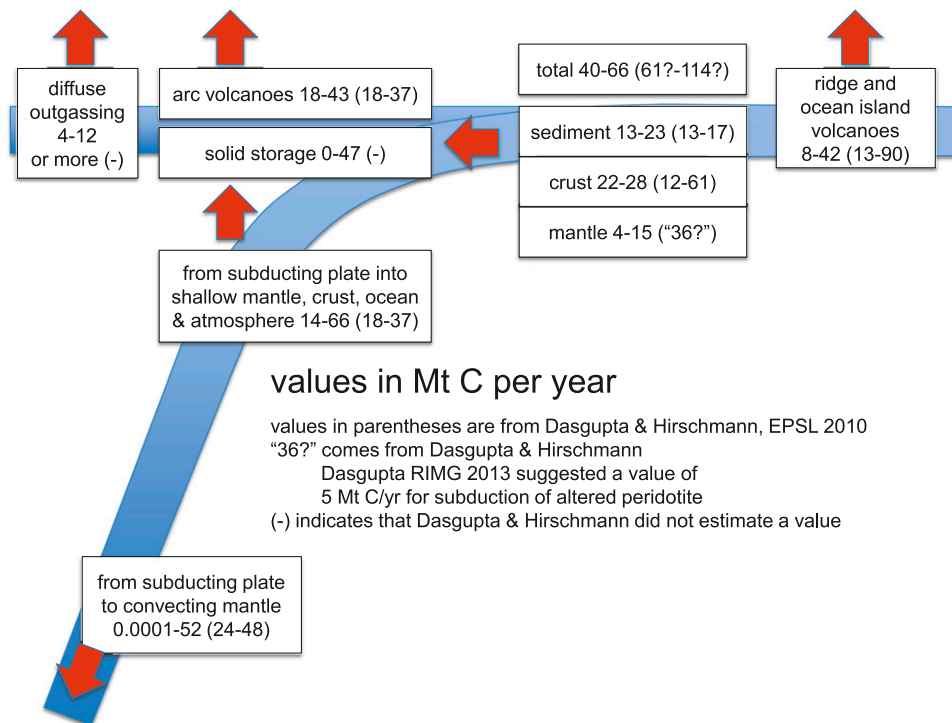


Fig. 5. Major fluxes of carbon estimated in this paper, with values from Dasgupta and Hirschmann (1) for comparison.

more examples in their studies of serpentine diapirs in the Mariana forearc (review in ref. 89).

Campbell et al. (90) list six other sites where active, diffuse outgassing of CO₂ and/or hydrocarbons has been detected in forearcs, and 10 more localities where evidence suggests that this happened in the past. In some cases, oxygen isotope data are indicative of derivation from a high-*T* source (e.g., refs. 91–93). However, unlike the Mariana seamounts, it is not clear in most cases how much carbon is derived from continental margin sedimentation, and from sediments in an accretionary prism, versus from subducting sediment.

There is venting of dense CO₂ liquid at hydrothermal sites on the flanks of submarine, Okinawa backarc and Mariana arc volcanoes (94–96). Because the water column in the Mariana arc has high, correlated CO₂/³He ratios indicative of significant, diffuse outgassing, Resing et al. (97) suggest global CO₂ fluxes from submarine volcanoes (based on CO₂/³He ratios and global ³He systematics) should be revised upward.

There are a few regional studies of diffuse CO₂ flux in arcs that can be used to make a global estimate. Both focus on magmatic CO₂ in spring water, in hot springs in the Taupo volcanic zone of New Zealand, and in both hot and cold springs in the Oregon Cascades. Seward and Kerrick (98) estimated a diffuse flux of 12 Mt C/y associated with Pacific Rim volcanism. For the central Oregon Cascades, James et al. (99) estimate a diffuse magmatic CO₂ degassing rate of 3.4 × 10⁵ kg/y per kilometer of arc, or about 4 Mt C/y over the 44,454 km of global subduction zones. We suspect that these values are underestimates.

Little Evidence for Storage in Arc Crust

In arc crustal sections, carbonate and calc–silicate veins formed at lower crustal and Moho depths have been observed, cross cutting arc plutonic rocks (100–105). These may provide important information on degassing from decompressing magmas, and/or from the complete crystallization of magmas at depth. However, such veins do not appear to be common.

Many intermediate to felsic plutonic rocks are liquids that underwent complete crystallization in arc middle crust (e.g., refs. 73, 106, and 107). If these magmas contained ~1.5 wt% CO₂ as inferred for intermediate arc magmas by Blundy et al. (86), their crystallization must have released substantial CO₂. Given the paucity of carbonate observed so far in oceanic arc middle and lower crust, this CO₂ must have been deposited within upper

crustal sedimentary and volcanic rocks, or emitted via diffuse outgassing (*Diffuse Outgassing of Carbon*).

Summary: A Likely Carbon Reservoir in the Mantle Lithosphere

Our average value of [C] in altered oceanic crust agrees with Alt and Teagle (15), but our compilation provides stronger constraints and clearer bounds on the uncertainty of this estimate. Similarly, [C] in samples of altered peridotites from the seafloor and ophiolites, together with seismic data on the depth and proportion of serpentinization at the outer rise, provides an improved constraint on [C] in subducting oceanic mantle. Consideration of organic carbon caused us to raise the upper bound for [C] in subducting sediments compared with Plank and coworkers (e.g., refs. 24 and 25). In sum, we estimate that subducting plates, including sediments, carry 39–66 Mt C/y into subduction zones.

Although listvenites formed by carbon mass transfer from subducting sediment into mantle peridotite at low *T* (<300 °C) are striking, we find that this flux and that in blueschist facies only account for transfer of 0–4 Mt C/y. Because carbonate solubility increases roughly along subduction zone geotherms, low-*PT* flux is much less important than carbon transport in eclogite facies at >550 °C.

Dissolution of carbonate from altered oceanic crust and sediments into migrating aqueous fluids in eclogite facies, combined with metamorphic decarbonation reactions, could transfer 4–59 Mt C/y into the hanging wall, for assumed bounds of 1–10 wt% fluid passing through the upper part of the subducting plate. In addition, metasedimentary layers more than ~100 m thick are likely to form buoyant diapirs, carrying much of the remaining sedimentary carbon into the mantle wedge at 700–900 °C. Melting of diapirs, subducting sediments and volcanics, and fluid-fluxed mantle peridotite will produce CO₂-bearing liquids that pass through the hot core of the mantle wedge and ascend into the overlying plate, precipitating carbonate minerals in mantle lithosphere and lower crust.

These considerations yield a total flux of 14–69 Mt C/y into arc lithosphere (forearc to backarc). Provided that fluid flow is diffusely distributed, dissolving most of the carbonate in altered oceanic crust, we expect that the correct flux is likely to be close to the maximum estimate, and that little carbon is recycled into the convecting mantle via subduction.

The upper bound is substantially higher than current estimates for combined volcanic and diffuse flux from arc systems into the ocean and atmosphere. Observed [C] in arc lower crust is small. If these values are correct, significant quantities of carbon are stored in the mantle lithosphere. Very large fluxes correspond to small [C], if carbon is distributed uniformly. For example, if arc mantle lithosphere is 20 km thick, extending from 50 km to 250 km from the trench, with an average age of 40 million years, then [C] of 1,000 ppm in this volume would correspond to precipitation of ~16 Mt C/y in the lithosphere. This is sufficient—together with output from arc volcanoes and diffuse venting—to balance the maximum estimated input of 69 Mt C/y into arc lithosphere. A campaign of geochemical analyses will be necessary to investigate the extent of a lithospheric mantle carbon reservoir. The residence time and long-term fate of carbon in such a reservoir is unclear. Much could remain in the continental upper mantle for billions of years, while some might return to the convecting mantle via delamination (108, 109).

Global Mass Balance

Global fluxes of carbon from Earth's interior to the surface, via magmatism at midocean ridges, within plate settings and arcs, plus diffuse fluxes, are highly uncertain. Marty et al. (110) reviewed and updated CO₂ output due to midocean ridge magmatism to reach an estimate of 8–21 Mt C/y. Similarly, Resing et al. (111) estimate a ridge flux of 6–24 Mt C/y. Marty and Tolstikhin (112) emphasized that the flux due to within-plate volcanism is uncertain, but is probably 10–100% of the ridge flux. The resulting range of values for combined carbon output from ridge and within-plate volcanism (8–42 Mt C/y) is reflected in Fig. 5 and discussed in *SI Text*.

Table 1. Summary of carbon flux estimates

Tectonic setting	Mt C/y	
	Min	Max
Total carbon input to subduction zones	40	66
Total outputs from subduction zones including fluid flux and solubility + metamorphic reactions + diapirs	14	66
Output to atmosphere at subaerial arc volcanoes	18	43
Diffuse output to ocean and atmosphere in arc systems	4	12 or more?
Storage in shallow, conductively cooled mantle ("lithosphere") and crust	0	47
Subducted carbon into convecting mantle	0.0001	52
Output to ocean and atmosphere at ridges and ocean islands	8	42

Most carbon is probably extracted from subducting plates via dissolution of carbonates in aqueous fluid, evolution of CO₂-rich fluid in metamorphic decarbonation reactions, and ascent in meta-sedimentary diapirs. In turn, most of this carbon will pass through the convecting mantle wedge and be returned to the mantle lithosphere, the crust, and—via volcanoes and diffuse outgassing—the oceans and the atmosphere. Thin metasedimentary layers, and some carbonate in altered oceanic crust, may continue to subduct into the deeper mantle, but this could involve a small fraction of total subducted carbon. Large changes in the influx of subducting carbon might lead to large changes in output. For example, if Cretaceous subduction zones were twice as long, and consumed thicker carbonate sediment sections (31), this probably produced more numerous and/or larger metasedimentary diapirs. Thus, temporal changes in subduction inputs and outputs are likely to be strongly correlated, whereas the rate of recycling of carbon into the convecting mantle may be nearly independent of the rate of input at subduction zones.

If the subduction zone carbon cycle is nearly balanced during subduction to 50–300 km depth (5–10 Ma), so that there is little recycling into the convecting mantle, and this has persisted over most of Earth history, then what about global fluxes of carbon out of the convecting mantle? Marty et al. (110) infer that most carbon output from midocean ridges and ocean islands is primordial carbon from “less-degassed” mantle reservoirs. If so, and if subduction zones return far less carbon to the convecting mantle than is extracted at ridges and ocean islands, then the proportion of carbon in the mantle lithosphere + crystalline crust + sediments + ocean + atmosphere must be increasing over time. Among these shallow reservoirs, carbon-bearing sediments and the mantle lithosphere are the most important.

Hayes and Waldbauer (27) reviewed [C] in continental crust, primarily in sediments. They estimated 10×10^{10} Mt carbon in the crust, intermediate between estimates from Holser et al. (113) and Wilkinson and Walker (114). In addition, if the upper 50 km of the mantle lithosphere contains 100–1,000 ppm carbon, for a continental area of 2.1×10^8 km² (115), this corresponds to $\sim 0.35\text{--}3.5 \times 10^{10}$ Mt C. Taking these estimates at face value, the continents (crust + mantle) contain $9.2\text{--}14.7 \times 10^{10}$ Mt C. Hayes and Waldbauer favor a nearly constant rate of growth of the continental crust (figure 7 in ref. 27), starting at 3.8 Ga. Thus, the net flux of CO₂ from the convecting mantle into the continents is 24–39 Mt C/y. These values are comparable to the estimates we summarized above, for midocean ridge plus within-plate fluxes, of 8–42 Mt C/y. Thus, it is plausible that ridge plus within-plate carbon output has caused a steady increase in the carbon inventory of the plates + oceans + atmosphere throughout Earth history, with very little recycling of carbon into the convecting mantle.

Carbon isotopes imply that at least 30% of diamonds contain recycled, sedimentary carbon (e.g., ref. 116). This recycled carbon may have been derived from fluids and/or melts carrying carbon from subducting sediment at 50–300 km within ~ 10 Ma of subduction, via processes described in this paper. However, a subset of diamonds—including some with inferred, recycled carbon—contain transition zone and lower mantle minerals. This suggests that some sedimentary carbon is indeed recycled into the convecting mantle on long time scales.

It is instructive to use diamond occurrences to place a lower bound on the flux of recycled sedimentary carbon into the convecting mantle. For the sake of argument, suppose that all diamonds, regardless of their carbon isotopes and mineral inclusions, formed from sedimentary carbon recycled into the convecting mantle. Most diamond occurrences are in kimberlite pipes. The probability that a kimberlite will be an economic diamond deposit is $\sim 0.5\%$ (117). The median concentration of diamonds in economic kimberlite deposits in 1992 was ~ 17 ppb. The average concentration in noneconomic kimberlites (less than 2 ppb in 1992, extending to zero) is negligible. Thus, taking the kimberlite data as representative

of the whole mantle, the concentration of diamond is 83 ppt, yielding 3×10^5 Mt of “recycled” carbon, approximately 300 thousand times smaller than the carbon inventory of the crust. This corresponds to recycling of $\sim 10^{-4}$ Mt C/y into the convecting mantle over 3.8 Ga.

Methods

Carbon concentrations in peridotite rock powders (Dataset S5) were measured with a Carbon Analyzer (LECO CS 844) with modules to determine total carbon (TC) and total inorganic carbon (TIC). For TC, samples in a ceramic boat were combusted in O₂ at $\sim 1,000$ °C. Evolved CO₂ in O₂ carrier gas was absorbed in a titration cell with ethanolamine and a colorimetric indicator. CO₂ concentration was determined via optical spectroscopy. For TIC, samples were titrated with perchloric acid and heated to 80 °C. Evolved CO₂ was measured as for TC. Samples previously analyzed by Schwarzenbach et al. (22) were analyzed to check accuracy and precision.

Conclusions: What Goes Down, Mostly Comes Up

Table 1 and Fig. 5 summarize fluxes estimated in this paper. Our upper-bound estimates indicate that almost all of the carbon in subducting sediments and oceanic plates may be extracted in fluids and melts that rise into the mantle wedge, and then—in buoyant solid diapirs and/or dissolved in fluids and melts—into the overlying plate. In contrast, previous reviews suggested that about half of subducting carbon is carried into the global, convecting mantle as part of the subducting oceanic plate.

When the influx of subducting carbon is larger than at present, it seems likely that the outflux will grow proportionately, so that balance between input and output may be maintained. If (i) our upper-bound estimates for carbon output from subducting plates are close to the actual fluxes, (ii) this carbon is transported through the mantle wedge into the mantle lithosphere and crust, and (iii) observed carbon output from volcanoes plus diffuse outgassing is smaller, then the mantle lithosphere is an important reservoir for carbon. Some carbon stored in the mantle lithosphere may eventually be recycled into the convecting mantle via delamination, while another component may remain indefinitely within the cratonic upper mantle.

Finally, if the subduction zone carbon cycle is approximately in balance, and if this is maintained over geologically significant times, then outgassing from midocean ridges and within-plate volcanic centers is not balanced and represents a net flux from the mantle to Earth’s surface. This possibility is broadly consistent with data on the carbon content of the continents, noble gas systematics, and constraints on the amount of recycled carbon incorporated in mantle diamonds.

Most of our estimates are highly uncertain. We lack quantitative data on [C] in key reservoirs. Additional data on the proportion and age of carbon-bearing minerals in eclogite facies and mantle wedge lithologies would be particularly valuable because this is the *PT* regime in which thermodynamic calculations yield the largest and most uncertain fluxes of carbon from the subducting plate into the mantle. We expect that data on [C] in high-grade metamorphic rocks and peridotites will become more abundant over the coming decade. Care will be needed to determine the timing and *PT* conditions during formation of carbon-bearing minerals in these settings because eclogites and wedge peridotites have surely been affected by other processes, before and after subduction zone metamorphism.

ACKNOWLEDGMENTS. We thank J. Ague, J. Connolly, R. Dasgupta, and D. Sverjensky for reviews; B. Hacker for joining a quixotic venture on Santa Catalina; M. Grove for spurring us on our way; the Two Tomos, Mizukami and Morishita, for hospitality in the Sanbagawa area; G. Bernasconi-Green for sharing data; T. Plank, R. Coggon, and D. Teagle for input on [C] in subducting materials; J. Alt and G. Harlow for sharing samples used as [C] standards; A. Hofmann, B. Marty, and M. Walter for advice on mantle carbon budgets; and H. Magunn, D. Vaccaro, and M. Stonor for carbon analyses. This research was supported by National Science Foundation Grants EAR-1049905 (to P.K.) and EAR-1347987 (to C.M.) and the Deep Carbon Observatory.

1. Dasgupta R, Hirschmann MM (2010) The deep carbon cycle and melting in Earth’s interior. *Earth Planet Sci Lett* 298:1–13.

2. Dasgupta R (2013) Ingressing, storage, and outgassing of terrestrial carbon through geologic time. *Rev Mineral Geochem* 75:183–229.

3. Alt JC, et al. (2013) The role of serpentinites in cycling of carbon and sulfur: Seafloor serpentinization and subduction metamorphism. *Lithos* 178:40–54.
4. Jarrard RD (2004) Subduction fluxes of water, carbon dioxide, chlorine, and potassium. *Geochem Geophys Geosyst* 4(5):8905.
5. Burton MR, Sawyer GM, Granieri D (2013) Deep carbon emissions from volcanoes. *Rev Mineral Geochem* 75:323–354.
6. Johnston FKB, Turchyn AV, Edmonds M (2011) Decarbonation efficiency in subduction zones: Implications for warm Cretaceous climates. *Earth Planet Sci Lett* 303:143–152.
7. Wallace PJ (2005) Volatiles in subduction zone magmas: Concentrations and fluxes based on melt inclusion and volcanic gas data. *J Volcanol Geotherm Res* 140:217–240.
8. Gorman PJ, Kerrick DM, Connolly JAD (2006) Modeling open system metamorphic decarbonation of subducting slabs. *Geochem Geophys Geosyst* 7(4):Q04007.
9. Kelemen PB, et al. (2011) Rates and mechanisms of mineral carbonation in peridotite: Natural processes and recipes for enhanced, in situ CO₂ capture and storage. *Annu Rev Earth Planet Sci* 39:545–576.
10. Fruh-Green GL, Connolly JAD, Plas A (2004) Serpentinization of oceanic peridotites: Implications for geochemical cycles and biological activity. *The Subseafloor Biosphere at Mid-Ocean Ridges*, eds Wilcock WSD, et al. (Am Geophys Union, Washington, DC), pp 119–136.
11. Manning CE, Shock EL, Sverjensky DA (2013) The chemistry of carbon in aqueous fluids at crustal and upper-mantle conditions: Experimental and theoretical constraints. *Rev Mineral Geochem* 75:109–148.
12. Manning CE (2013) Thermodynamic modeling of fluid-rock interaction at mid-crustal to upper mantle conditions. *Rev Mineral Geochem* 76:135–164.
13. Van Avendonk HJA, Holbrook WS, Lizarralde D, Denyer P (2011) Structure and serpentinization of the subducting Cocos plate offshore Nicaragua and Costa Rica. *Geochem Geophys Geosyst* 12(6):Q06009.
14. Behn MD, Kelemen PB, Hirth G, Hacker BR, Massonne HJ (2011) Diapirs as the source of the sediment signature in arc lavas. *Nat Geosci* 4:641–646.
15. Alt JC, Teagle DAH (1999) The uptake of carbon during alteration of oceanic crust. *Geochim Cosmochim Acta* 63:1527–1535.
16. Carlson RL (2001) The abundance of ultramafic rocks in the Atlantic Ocean crust. *Geophys J Int* 144:37–48.
17. Cannat M, et al. (1995) Thin crust, ultramafic exposure and rugged faulting patterns at the Mid-Atlantic Ridge (22°–24°N). *Geology* 23:49–52.
18. DeMets C, Gordon RG, Argus DF, Stein S (1990) Current plate motions. *Geophys J Int* 101:425–478.
19. Bird P (2003) An updated digital model of plate boundaries. *Geochem Geophys Geosyst* 4(3):1027.
20. Alt JC, et al. (2012) Uptake of carbon and sulfur during seafloor serpentinization and the effects of subduction metamorphism in Ligurian peridotites. *Chem Geol* 322-323:268–277.
21. Alt JC, et al. (2012) Recycling of water, carbon, and sulfur during subduction of serpentinites: A stable isotope study of Cerro del Almirez, Spain. *Earth Planet Sci Lett* 327-328:50–60.
22. Schwarzenbach EM, Fruh-Green GL, Bernasconi SM, Alt JC, Plas A (2013) Serpentinization and carbon sequestration: A study of two ancient peridotite-hosted hydrothermal systems. *Chem Geol* 351:115–133.
23. Rea DK, Ruff LJ (1996) Composition and mass flux of sediment entering the world's subduction zones: Implications for global sediment budgets, great earthquakes, and volcanism. *Earth Planet Sci Lett* 140:1–12.
24. Plank T, Langmuir CH (1998) The chemical composition of subducting sediment and its consequences for the crust and mantle. *Chem Geol* 145:325–394.
25. Plank T (2014) The chemical composition of subducting sediments. *The Crust*, Treatise on Geochemistry, ed Rudnick RL (Elsevier-Pergamon, Oxford), 2nd Ed, Vol 4, pp 607–629.
26. Mayer L, Piasias N, Janacek T (1992) *Proceedings of the Ocean Drilling Program, Initial Reports* (Ocean Drill Program, College Station, TX), Vol 138.
27. Hayes JM, Waldbauer JR (2006) The carbon cycle and associated redox processes through time. *Philos Trans R Soc Lond B Biol Sci* 361(1470):931–950.
28. Ridgwell A (2005) A mid Mesozoic revolution in the regulation of ocean chemistry. *Mar Geol* 217:339–357.
29. Falkowski PG, et al. (2004) The evolution of modern eukaryotic phytoplankton. *Science* 305(5682):354–360.
30. Winterer EL (2001) The oldest biogenous pelagic sediments above Mesozoic oceanic basement: A review. *Paradoxes in Geology*, eds Briegel U, Xiao W (Elsevier, Amsterdam), pp 373–385.
31. Lee C-TA, et al. (2013) Continental arc–island arc fluctuations, growth of crustal carbonates, and long-term climate change. *Geosphere* 9:21–36.
32. Caldwell JG, Haxby WF, Karig DE, Turcotte DL (1976) Applicability of a universal elastic trench profile. *Earth Planet Sci Lett* 31:239–246.
33. Chapple WM, Forsyth DW (1979) Earthquakes and bending of plates at trenches. *J Geophys Res* 84:6729–6749.
34. Shillington DJ, et al. (2014) Controls on abrupt changes in faulting, hydration and seismicity in the Alaska subduction zone. *Nature*, in press.
35. Kerrick DM, Connolly JAD (2001) Metamorphic devolatilization of subducted oceanic metabasalts: Implications for seismicity, arc magmatism and volatile recycling. *Earth Planet Sci Lett* 189:19–29.
36. Falk ES, Kelemen PB (2015) Geochemistry and petrology of listvenite in the Somali ophiolite, Sultanate of Oman: Complete carbonation of peridotite during ophiolite emplacement. *Geochim Cosmochim Acta* 160:70–90.
37. Boudier F, et al. (1985) Kinematics of oceanic thrusting in the Oman ophiolite: Model of plate convergence. *Earth Planet Sci Lett* 75:215–222.
38. Hacker BR, Gnos E (1997) The conundrum of Samail: Explaining the metamorphic history. *Tectonophysics*. 279:215–226.
39. Syracuse EM, van Keken PE, Abers GA (2010) The global range of subduction zone thermal models. *Phys Earth Planet Inter* 183:73–90.
40. Wada I, Wang K (2009) Common depth of slab-mantle decoupling: Reconciling diversity and uniformity of subduction zones. *Geochem Geophys Geosyst* 10(10):Q10009.
41. Bond GC, Kominz MA (1984) Construction of tectonic subsidence curves for the early Paleozoic miogeocline, southern Canadian Rocky Mountains: Implications for subsidence mechanisms, age of breakup, and crustal thinning. *Geol Soc Am Bull* 95:155–173.
42. Lynch FL (1997) Frio shale mineralogy and the stoichiometry of the smectite-to-illite reaction: The most important reaction in clastic sedimentary diagenesis. *Clays Clay Miner* 45:618–631.
43. Grove M, et al. (2008) The Catalina Schist: Evidence for middle Cretaceous subduction erosion of southwestern North America. *Spec Pap Geol Soc Am* 436:335–361.
44. Bebout GE, Barton MD (1989) Fluid flow and metasomatism in a subduction zone hydrothermal system: Catalina Schist terrane. *Calif Geol* 17:976–980.
45. Bebout GE, Barton MD (1993) Metasomatism during subduction: Products and possible paths in the Catalina Schist, California. *Chem Geol* 108:61–92.
46. Naldrett AJ (1966) Talc-carbonate alteration of some serpentinized ultramafic rocks south of Timmins, Ontario. *J Petrol* 7:489–499.
47. Schandl ES, Naldrett AJ (1992) CO₂ metasomatism of serpentinites south of Timmins, Ontario. *Can Mineral* 30:93–108.
48. Ague JJ, Nicolescu S (2014) Carbon dioxide released from subduction zones by fluid-mediated reactions. *Nat Geosci* 7:355–360.
49. Sverjensky DA, Harrison B, Azzolini D (2014) Water in the deep Earth: The dielectric constant and the solubilities of quartz and corundum to 60kb and 1200° C. *Geochim Cosmochim Acta* 129:125–145.
50. Façq S, Daniel I, Montagnac G, Cardon H, Sverjensky DA (2014) In situ Raman study and thermodynamic model of aqueous carbonate speciation in equilibrium with aragonite under subduction zone conditions. *Geochim Cosmochim Acta* 132:375–390.
51. Newton RC, Manning CE (2002) Experimental determination of calcite solubility in H₂O-NaCl solutions at deep crust/upper mantle pressures and temperatures: Implications for metasomatic processes in shear zones. *Am Mineral* 87:1401–1409.
52. Lazar C, Young ED, Manning CE (2012) Experimental determination of equilibrium nickel isotope fractionation between metal and silicate from 500 °C to 950 °C. *Geochim Cosmochim Acta* 86:276–295.
53. Cook-Kollars J, Bebout GE, Collins NC, Angiboust S, Agard P (2014) Subduction zone metamorphic pathway for deep carbon cycling: I. Evidence from HPU/UHP metasedimentary rocks, Italian Alps. *Chem Geol* 386:31–48.
54. Aoya M, Endo S, Mizukami T, Wallis SR (2013) Paleo-mantle wedge preserved in the Sambagawa high-pressure metamorphic belt and the thickness of forearc continental crust. *Geology* 41:451–454.
55. Endo S, Tsuboi M (2013) Petrogenesis and implications of jadeite-bearing kyanite eclogite from the Sanbagawa belt (SW Japan). *J Metamorph Geol* 31:647–661.
56. Enami M, Mizukami T, Yokoyama K (2004) Metamorphic evolution of garnet-bearing ultramafic rocks from the Gongen area, Sanbagawa belt, Japan. *J Metamorph Geol* 22:1–15.
57. Hirai H, Arai S (1987) H₂O-CO₂ fluids supplied in alpine-type mantle peridotites: Electron petrology of relic fluid inclusions in olivines. *Earth Planet Sci Lett* 85:311–318.
58. Arai S, Ishimaru S, Mizukami T (2012) Methane and propane micro-inclusions in olivine in titanoclinohumite bearing dunites from the Sanbagawa high-P metamorphic belt, Japan: Hydrocarbon activity in a subduction zone and Ti mobility. *Earth Planet Sci Lett* 353-354:1–11.
59. Aoki K, et al. (2009) Metamorphic P–T–time history of the Sanbagawa belt in central Shikoku, Japan and implications for retrograde metamorphism during exhumation. *Lithos* 113:393–407.
60. Frezzotti ML, Selverstone J, Sharp ZD, Compagnoni R (2011) Carbonate dissolution during subduction revealed by diamond-bearing rocks from the Alps. *Nat Geosci* 4:703–706.
61. Hacker BR (2008) H₂O subduction beyond arcs. *Geochem Geophys Geosyst* 9(3):Q03001.
62. van Keken PE, Hacker BR, Syracuse EM, Abers GA (2011) Subduction factory: 4. Depth-dependent flux of H₂O from subducting slabs worldwide. *J Geophys Res* 116(B1):B01401.
63. Kerrick DM (2001) Present and past nonanthropogenic CO₂ degassing from the solid earth. *Rev Geophys* 39:565–585.
64. Kerrick DM, Connolly JAD (1998) Subduction of opicarbonates and recycling of CO₂ and H₂O. *Geology* 26(4):375–378.
65. Galvez ME, Manning CE, Connolly JAD, Rumble D (2015) The solubility of rocks in metamorphic fluids: Theory and example of graphite-bearing pelite to 900 °C and 3 GPa. *Earth Planet Sci Lett*, in press.
66. Mysen BO, Wheeler K (2000) Solubility behavior of water in haploandesitic melts at high pressure and high temperature. *Am Mineral* 85:1128–1142.
67. Kawamoto T, Holloway JR (1997) Melting temperature and partial melt chemistry of H₂O-saturated mantle peridotite to 11 Gigapascals. *Science* 276(5310):240–243.
68. Duncan MS, Dasgupta R (2014) CO₂ solubility and speciation in rhyolitic sediment partial melts at 1.5–3.0 GPa – Implications for carbon flux in subduction zones. *Geochim Cosmochim Acta* 124:328–347.
69. Schmidt MW, Vielzeuf D, Auzanneau E (2004) Melting and dissolution of subducting crust at high pressures: The key role of white mica. *Earth Planet Sci Lett* 228:65–84.
70. Mallik A, Dasgupta R (2013) Reactive infiltration of MORB-eclogite-derived carbonated silicate melt into fertile peridotite at 3 GPa and genesis of alkalic magmas. *J Petrol* 53:2267–2300.
71. Mallik A, Dasgupta R (2012) Reaction between MORB-eclogite derived melts and fertile peridotite and generation of ocean island basalts. *Earth Planet Sci Lett* 329-330:97–108.

72. Mallik A, Dasgupta R (2014) Effect of variable CO₂ on eclogite-derived andesite and lherzolite reaction at 3 GPa—Implications for mantle source characteristics of alkalic ocean island basalts. *Geochem Geophys Geosyst* 15:1533–1557.
73. Kelemen PB, Hanghøj K, Greene A (2003) One view of the geochemistry of subduction-related magmatic arcs, with an emphasis on primitive andesite and lower crust. *The Crust, Treatise on Geochemistry*, ed Rudnick RL (Elsevier-Pergamon, Oxford), Vol 3, pp 593–659.
74. Tsuno K, Dasgupta R, Danielson L, Richter K (2012) Flux of carbonate melt from deeply subducted pelitic sediments: Geophysical and geochemical implications for the source of Central American volcanic arc. *Geophys Res Lett* 39(16):L16307.
75. Tsuno K, Dasgupta R (2011) Melting phase relation of nominally anhydrous, carbonated pelitic-eclogite at 2.5–3.0 GPa and deep cycling of sedimentary carbon. *Contrib Mineral Petrol* 161:743–763.
76. Marschall HR, Schumacher JC (2012) Arc magmas sourced from mélange diapirs in subduction zones. *Nat Geosci* 5:862–867.
77. Wyllie PJ, Huang W-L (1976) Carbonation and melting reactions in the system CaO-MgO-SiO₂-CO₂ at mantle pressures with geophysical and petrological applications. *Contrib Mineral Petrol* 54:79–107.
78. Dasgupta R, Hirschmann MM, Smith ND (2007) Water follows carbon: CO₂ incites deep silicate melting and dehydration beneath mid-ocean ridges. *Geology* 35(2):135–138.
79. Dasgupta R, Hirschmann MM (2006) Melting in the Earth's deep upper mantle caused by carbon dioxide. *Nature* 440(7084):659–662.
80. Sharp ZD, Essene EJ, Smyth JR (1992) Ultra-high temperatures from oxygen isotope thermometry of a coesite-sandine grosspyrite. *Contrib Mineral Petrol* 112:358–370.
81. Shimoda G, Tatsumi Y, Nohda S, Ishizaka K, Jahn BM (1998) Setouchi high-Mg andesites revisited: Geochemical evidence for melting of subducting sediments. *Earth Planet Sci Lett* 160:479–492.
82. Newton RC (1992) Charnockitic alteration: Evidence for CO₂ infiltration in granulite facies metamorphism. *J Metamorph Geol* 10:383–400.
83. Newton RC, Aranovich LY, Hansen EC, Vandenheuvell BA (1998) Hypersaline fluids in Precambrian deep-crustal metamorphism. *Precambrian Res* 91:41–63.
84. Manning CE, Aranovich LY (2014) Brines at high pressure and temperature: Thermodynamic, petrologic and geochemical effects. *Precambrian Res* 253:6–16.
85. Hilton DR, Fischer TP, Marty B (2002) Noble gases and volatile recycling at subduction zones. *Rev Mineral* 47:319–370.
86. Blundy J, Cashman KV, Rust A, Witham F (2010) A case for CO₂-rich arc magmas. *Earth Planet Sci Lett* 290:289–301.
87. Morner N-A, Etiope G (2002) Carbon degassing from the lithosphere. *Global Planet Change* 33:185–203.
88. Haggerty JA (1987) Petrology and geochemistry of Neogene sedimentary rocks from Mariana forearc seamounts: Implications for origin of the seamounts. *Seamounts, Islands, and Atolls*, eds Keating BH, Fryer P, Batiza R, Boehlert GW (Am Geophys Union, Washington, DC), pp 175–185.
89. Fryer P (2012) Serpentinite mud volcanism: Observations, processes, and implications. *Annu Rev Mar Sci* 4:345–373.
90. Campbell KA, Farmer JD, Des Marais D (2002) Ancient hydrocarbon seeps from the Mesozoic convergent margin of California: Carbonate geochemistry, fluids and palaeoenvironments. *Geofluids* 2:63–94.
91. Kulm LD, Suess E (1990) Relationship between carbonate deposits and fluid venting: Oregon Accretionary Prism. *J Geophys Res* 95:8899–8915.
92. Kulm LD, et al. (1986) Oregon subduction zone: Venting, fauna, and carbonates. *Science* 231(4738):561–566.
93. Sample JC (1996) Isotopic evidence from authigenic carbonates for rapid upward fluid flow in accretionary wedges. *Geology* 24:897–900.
94. Lupton J, et al. (2006) Submarine venting of liquid carbon dioxide on a Mariana Arc volcano. *Geochem Geophys Geosyst* 7(8):Q08007.
95. Sakai H, et al. (1990) Venting of carbon dioxide-rich fluid and hydrate formation in mid-Okinawa Trough backarc basin. *Science* 248(4959):1093–1096.
96. Konno U, et al. (2006) Liquid CO₂ venting on the seafloor: Yonaguni Knoll IV hydrothermal system, Okinawa Trough. *Geophys Res Lett* 33(16):L16607.
97. Resing JA, et al. (2009) Chemistry of hydrothermal plumes above submarine volcanoes of the Mariana Arc. *Geochem Geophys Geosyst* 10(2):Q02009.
98. Seward TM, Kerrick DM (1996) Hydrothermal CO₂ emission from the Taupo Volcanic Zone, New Zealand. *Earth Planet Sci Lett* 139:105–113.
99. James ER, Manga M, Rose TP, Hudson GB (2000) The use of temperature and the isotopes of O, H, C, and noble gases to determine the pattern and spatial extent of groundwater flow. *J Hydrol* 237:100–112.
100. Hacker BR, et al. (2008) Reconstruction of the Talkeetna intraoceanic arc of Alaska through thermobarometry. *J Geophys Res* 113(B3):B03204.
101. Bradshaw JY (1989) Early Cretaceous vein-related garnet granulite in Fiordland, southwest New Zealand: A case for infiltration of mantle-derived CO₂-rich fluids. *J Geol* 97:697–717.
102. Blattner P, Black PM (1980) Apatite and scapolite as petrogenetic indicators in granulites of Milford Sound, New Zealand. *Contrib Mineral Petrol* 74:339–348.
103. Yoshino T, Satish-Kumar M (2001) Origin of scapolite in deep-seated metagabbros of the Kohistan arc, NW Himalaya. *Contrib Mineral Petrol* 140:511–531.
104. Bouilhol P, Burg JP, Bodinier JL (2012) Gem olivine and calcite mineralization precipitated from subduction-derived fluids in the Kohistan arc-mantle (Pakistan). *Can Mineral* 50:1291–1304.
105. Bouilhol P, Burg JP, Bodinier JL, Schmidt MW (2009) Magma and fluid percolation in arc to forearc mantle: Evidence from Sapat (Kohistan, Northern Pakistan). *Lithos* 107:17–37.
106. Kelemen PB, Hanghøj K, Greene AR (2014) One view of the geochemistry of subduction-related magmatic arcs with an emphasis on primitive andesite and lower crust. *The Crust, Treatise on Geochemistry*, ed Rudnick RL (Elsevier-Pergamon, Oxford), 2nd Ed, Vol. 4, pp 749–806.
107. Jagoutz O, Schmidt M (2012) The formation and bulk composition of modern juvenile continental crust: The Kohistan arc. *Chem Geol* 298-299:79–96.
108. Houseman GA, McKenzie DP, Molnar P (1981) Convective instability of a thickened boundary layer and its relevance for the thermal evolution of continental convergent belts. *J Geophys Res* 86:6115–6132.
109. Houseman GA, Molnar P (1997) Gravitational (Rayleigh-Taylor) instability of a viscosity and convective thinning of continental layer with non-linear lithosphere. *Geophys J Int* 128:125–150.
110. Marty B, Alexander CMOD, Raymond S (2013) Primordial origins of Earth's carbon. *Rev Mineral Geochem* 75:149–181.
111. Resing JA, Lupton JE, Feely RA, Lilley MD (2004) CO₂ and ³He in hydrothermal plumes: Implications for Mid-Ocean Ridge CO₂ flux. *Earth Planet Sci Lett* 226:449–464.
112. Marty B, Tolstikhin IN (1998) CO₂ fluxes from mid-ocean ridges, arcs and plumes. *Chem Geol* 145:233–248.
113. Holser WT, Schidlowski M, MacKenzie FT, Maynard JB (1988) Geochemical cycles of carbon and sulfur. *Chemical Cycles in the Evolution of the Earth*, eds Gregor CB, Garrels RM, Mackenzie FT, Maynard JB (Wiley, New York), pp 105–173.
114. Wilkinson BH, Walker JCG (1989) Phanerozoic cycling of sedimentary carbonate. *Am J Sci* 289:525–548.
115. Cogley JG (1984) Continental margins and the extent and number of the continents. *Rev Geophys* 22:101–122.
116. Shirey SB, et al. (2013) Diamonds and the geology of mantle carbon. *Rev Mineral Geochem* 75:355–421.
117. Bliss JD (1992) Grade-tonnage and other models for diamond kimberlite pipes. *Nonrenewable Resour* 1:214–230.
118. Ulmer P, Trommsdorff V (1995) Serpentine stability to mantle depths and subduction-related magmatism. *Science* 268(5212):858–861.
119. Falloon TJ, Green DH (1989) The solidus of carbonated, fertile peridotite. *Earth Planet Sci Lett* 94:364–370.